#### Glaucoma

## Perimetric Stimuli Undergoing Complete Spatial Summation Optimize the Detection of Retinal Ganglion Cell Density Gradients in Healthy Observers

Caitlín S. Campbell<sup>1,2</sup>, Victoria Stapley<sup>1</sup>, Roger S. Anderson<sup>1,2</sup>, David F. Garway-Heath<sup>2</sup>, Tony Redmond<sup>3</sup>, and Pádraig J. Mulholland<sup>1-3</sup>

- <sup>1</sup> Centre for Optometry & Vision Science, Biomedical Sciences Research Institute, Ulster University, Coleraine, Northern Ireland, UK
- <sup>2</sup> National Institute for Health & Care Research (NIHR) Biomedical Research Centre at Moorfields Eye Hospital NHS Foundation Trust and UCL Institute of Ophthalmology, London, UK

Correspondence: Pádraig Mulholland, Ulster University, Cromore Rd., Coleraine BT52 1SA, Northern Ireland, UK. e-mail: p.mulholland@ulster.ac.uk

Received: August 11, 2025 Accepted: September 22, 2025 Published: November 13, 2025

**Keywords:** retinal ganglion cell; spatial summation; area modulation stimuli; perimetry; glaucoma

Citation: Campbell CS, Stapley V, Anderson RS, Garway-Heath DF, Redmond T, Mulholland PJ. perimetric stimuli undergoing complete spatial summation optimize the detection of retinal ganglion cell density gradients in healthy observers. Transl Vis Sci Technol. 2025;14(11):14, https://doi.org/10.1167/tvst.14.11.14 **Purpose:** To compare the ability of conventional luminance-modulating perimetric stimuli and an area-modulation stimulus (AMS) designed to measure changes in complete spatial summation to identify physiological retinal ganglion cell density (RGCD) gradients in healthy observers.

**Methods:** Contrast thresholds were measured for Goldmann III (GIII; 0.43°, 200 ms) and V (GV; 1.72°, 200 ms) stimuli at 3° and 10° eccentricity in 100 healthy observers (median age, 43 years, range, 18–85 years), with mean spherical equivalent refractive errors ranging from -10.38 to +4.63 DS. Area thresholds were measured at the same locations using a fixed luminance stimulus ( $\Delta$ L: 4.4 cd/m², 200 ms). Colocalized RGCD estimates were determined using (i) optical coherence tomography (OCT) RGC layer thickness measures, and (ii) achromatic peripheral grating resolution acuity (PGRA) thresholds. Ratios of the difference in log energy threshold ( $\Delta$ E) and log RGCD ( $\Delta$ RGCD) between eccentricities were calculated ( $\Delta$ E/| $\Delta$ RGCD|), with a value of 1 assumed to be the optimal relationship between functional thresholds and RGCD.

**Results:**  $\Delta$ E/ $|\Delta$ RGCD|) values (median and interquartile range [IQR]) were largest for AMS (OCT, 0.54 [IQR, 0.37–0.78]; PGRA, 0.71 [IQR, 0.46–1.19]), followed by GIII (OCT, 0.29 [IQR, 0.08–0.44]; PGRA, 0.33 [IQR, 0.07–0.54]; and GV (OCT, 0.16 [IQR, 0.02–0.29]; and PGRA, 0.19 [IQR, 0.02–0.44]). Interstimulus differences between all stimulus pairs were statistically significant (AMS vs GIII, both P < 0.001; AMS vs GV, both P < 0.001; GIII vs GV, both P < 0.05).

**Conclusions:**  $\Delta E/|\Delta RGCD|$  values were closest to 1 for AMS, suggesting this stimulus relates best to underlying physiological variations in RGCD.

**Translational Relevance:** Thresholds measured with area modulation stimuli vary more proportionally with physiological changes in retinal ganglion cell density relative to conventional perimetric stimuli.

## Introduction

Standard automated perimetry (SAP) is the reference standard test for the detection and monitoring of visual function loss associated with the death of retinal ganglion cells (RGCs) in glaucoma.<sup>1</sup> Although the test is widely adopted for this purpose, previous

work has shown that SAP sensitivity has a shallow and variable relationship with RGC density (RGCD) that varies with visual field eccentricity,<sup>2–4</sup> glaucoma disease stage,<sup>5</sup> and stimulus area.<sup>6</sup> Much of this variation in the relationship between RGCD and SAP thresholds can be attributed to differences in the extent of spatial summation that determines threshold for the fixed area Goldmann stimuli (GI–GV, 0.11°–1.72° diame-

Copyright 2025 The Authors tvst.arvojournals.org | ISSN: 2164-2591



<sup>&</sup>lt;sup>3</sup> School of Optometry and Vision Sciences, Cardiff University, Cardiff, UK

ter) used. Specifically, the commonly used GIII stimulus has been shown to be larger than the upper limit of complete spatial summation (Ricco's area [RA]) in healthy observers at many test locations within the central 24° of the visual field, which may be responsible for a shallow relationship between RGCD and SAP thresholds. At more peripheral locations, the relationship between RGCD and SAP thresholds approximates 1:1. In this region, the fixed area GIII stimulus is smaller than RA and thresholds are determined by complete spatial summation. Thus, spatial summation is likely to play an important role in the relationship between perimetric sensitivity and underlying retinal structure.

Given that RA enlarges as a function of physiological (e.g., with visual field/retinal eccentricity,11 axial myopia<sup>12</sup>), and pathological (e.g., glaucoma<sup>7,9,10</sup>) alterations in RGCD, it is hypothesized that, with a stimulus that thresholds by self-scaling to the localized RA, a more uniform 1:1 relationship between perimetric thresholds and RGCD would be observed. Our group has previously described the use of an area modulating stimulus (AMS) that scales to the localized RA in glaucoma. 10,13 This stimulus displayed a greater glaucoma disease signal, more uniform response variability with depth of defect, and a higher ratio of disease signal to measurement variability (noise) when compared with conventional SAP stimuli modulating in luminance.<sup>13</sup> To date, no study has examined the structure-function relationship between AMS thresholds and underlying RGCD in regions of healthy eyes where high interindividual variations in RGCD are known to occur. 14 Examining this relationship in a cohort of healthy observers will permit the true underlying nature of this relationship to be examined in the absence of confounding effects that can occur in disease (e.g., increased measurement variability for structural and functional measures, RGC dysfunction). Because AMS holds promise for greater utility in the detection and monitoring of glaucoma, it is essential to understand how physiological variances in underlying RGCD relate to AMS functional thresholds. In addition to forming a baseline understanding of structure–function relationships in healthy eyes, such information would also have importance for disentangling physiological variations in RGCD (and thus spatial summation), as can occur in axially myopic eyes<sup>12</sup> from pathological changes in glaucoma.

In this study, we investigated whether sensitivity measures with an achromatic AMS designed to scale to the local RA at threshold have a greater association with physiological gradients in RGCD calculated using RGC estimates derived from structural [optical coherence tomography (OCT)] and functional [peripheral

grating resolution acuity (PGRA)] data that occur with eccentricity in healthy observers relative to conventional perimetric stimuli (GIII and GV) modulating in luminance. We also describe a novel method to evaluate the relationship between functional psychophysical thresholds collected using these stimuli (AMS, GIII, and GV) and physiological gradients in RGCD that occur with eccentricity<sup>14</sup> and/or axial elongation<sup>12,15–17</sup> in healthy observers.

### **Methods**

#### **Participants**

One hundred healthy observers, including 49 myopes (median age, 35 years; range, 18–85 years) and 51 age-similar (Mann–Whitney U test, P = 0.71) nonmyopic controls (median age, 51 years; range, 18–76 years) participated in this study. All participants had a best corrected monocular distance visual acuity of 0.20 logarithm of the minimum angle of resolution (logMAR) (6/9, 20/30) or better (median, -0.10logMAR; range, -0.20 to 0.12 logMAR) and a full visual field in the test eye (median, 0.23; interquartile range [IOR], -0.40 to 0.85), as measured with the 24-2 SITA Standard threshold test (Humphrey Visual Field Analyzer, Carl Zeiss Meditec, Dublin, CA). All participants had intraocular pressures between 11 and 21 mm Hg measured with Goldmann applanation tonometry and no significant media opacities or ocular disease as determined by a UK-qualified optometrist using slit-lamp assessment of the anterior eye and biomicroscopic posterior segment examination. For all participants, peripapillary retinal nerve fiber layer and macular OCT scans ( $30^{\circ} \times 25^{\circ}$  cube; 61 B-scans; automatic real-time tracking, 9; tilted to account for fovea-optic nerve axis) revealed no abnormalities (Spectralis OCT, Heidelberg Engineering, Heidelberg, Germany). No participant was diagnosed with a systemic condition or took medication that could have influenced vision. All participants were recruited and tested at the Centre for Optometry and Vision Science at Ulster University.

Refractive error was measured objectively using a binocular open-field autorefractor (Shin Nippon NVision-K 5001, Shin-Nippon, Tokyo, Japan), this being subjectively refined to determine a final refractive error. For all participants, astigmatism was less than 3.50 DC in the test eye. Refractive error was expressed as mean spherical equivalent, with myopia defined as a mean spherical equivalent of -0.50 DS or less. Refractive error ranged from -0.50 DS to -10.38 DS in the myopic group and from -0.25 DS to +4.63 DS

**Table 1.** Summary Characteristics of the Myopic and Nonmyopic Groups

	Myopic Group ( $n = 49$ )	Nonmyopic Group ( $n = 51$ )	
Age (years)	Median, 35	Median, 51	
	(Range:18 to 85)	(Range: 18 to 76)	
	(IQR: 23 to 57)	(IQR: 20 to 64)	
Refractive error MSE (DS)	Median, —2.75	Median, $+0.25$	
	(Range: $-0.50$ to $-10.38$ )	(Range: $-0.25$ to $+4.63$ )	
	(IQR: -1.59  to  -5.62)	(IQR: +0.13  to  +1.28)	
Astigmatism (DC)	Median, $-0.75$	Median, -0.50	
	(Range: $0.00 \text{ to } -3.25$ )	(Range: $0.00 \text{ to } -2.50$ )	
	(IQR: -0.25 to -1.25)	(IQR: -0.25 to -0.75)	
AL (mm)	Median, 24.55	Median, 23.34	
	(Range: 22.89 to 27.96)	(Range: 21.38 to 25.42)	
	(IQR: 23.68 to 26.03)	(IQR: 22.90 to 23.62)	

MSE, mean spherical equivalent.

in the nonmyopic control group. Based on the International Myopia Institute (IMI, 2019) definitions, <sup>18</sup> 11 participants (22.4%) in the myopic group were defined as high myopes ( $\leq$ -6.00 DS), with the remainder (n = 38 [77.6%]) having myopia in the range -0.50 to -5.75 DS (low to moderate myopes). Axial length (AL) was recorded as the average of five measures with the IOLMaster 700 (Carl Zeiss Meditec). Participant characteristics for each group are displayed in Table 1.

Ethical approval for this study was granted by the Ulster University Biomedical Sciences Research Ethics Filter Committee. Informed, written consent was obtained from all participants before data collection, and this research adhered to the tenets of the Declaration of Helsinki.

### **Apparatus and Stimuli**

Stimuli were generated using MATLAB (2021b, The MathWorks, Natick, MA) with Psychtoolbox (v3.0) and a Bits# (Cambridge Research Systems, Rochester, UK) and presented on a gamma-corrected cathode ray tube display (SONY 420GS, Tokyo, Japan; pixel resolution of  $1280 \times 1024$ ; refresh rate of 60 Hz) after a minimum warm-up period of 1 hour. An annulus fixation target (white 0.45° diameter spot with a central zero-contrast 0.23° diameter spot) was used for all tests. Participant responses were collected with a Cedrus RB-540 response pad (Cedrus Corporation, Los Angeles, CA). Stimuli were presented at two test locations, one at 3° and one at 10° eccentricity, both along the 45° meridian in the inferonasal quadrant of the visual field, with stimuli also being presented at four distractor locations spread across other meridians and eccentricities (3°-15°) to minimize attentional bias. A viewing distance of 62 cm was used for all tests. Participants were optically corrected for this specific test distance using full aperture trial lenses placed at the anterior focal point of the eye (vertex distance of 15.2 mm). This vertex distance was selected to satisfy Knapp's law, such that the retinal image size remained constant with varying axial ametropia. <sup>12,19</sup> Astigmatism was corrected if greater than 1.00 DC; otherwise, the mean spherical equivalent was used. Participants placed their head on a purpose-built forehead and chinrest, with their nontested eye occluded with an opaque eye patch.

Data were collected within four psychophysical tests (see Psychophysical Procedure), with the order of tests being randomized for each participant but referred to below as tests 1 through 4 for ease of explanation. Rest periods were provided at regular intervals after each test and upon the participant's request. In test 1, area thresholds were measured using an achromatic circular area-modulating stimulus of fixed duration (Bridgeman<sup>20</sup> duration of 184.5 ms, 12 frames) and luminance ( $\Delta I$ , 4.4 cd/m<sup>2</sup>; log  $\Delta L/L$ , -0.30), based on the expected contrast threshold for a RA-scaled luminance-modulated stimulus under the same conditions in healthy observers. 7,11,13,21 In tests 2 and 3, contrast thresholds were measured for GIII (0.14 deg<sup>2</sup>) and GV (2.32 deg<sup>2</sup>) equivalent stimuli (Bridgeman<sup>22</sup> duration of 184.5 ms; reference standard SAP stimuli), respectively. For tests 1, 2, and 3, a uniform gray background of mean luminance 9.60 cd/m<sup>2</sup> was used, with chromaticity coordinates of the background and stimuli measured as x = 0.284 and y = 0.290 using a colorimeter (ColorCAL-II, Cambridge Research Systems, Rochester, UK). In test 4, PGRA was measured for an achromatic Gabor stimulus (sinephase, SD\*spatial frequency = 4; Michelson contrast 99%; mean and background luminance 30 cd/m<sup>2</sup> [within Weber's region<sup>22</sup>]; Bridgeman<sup>22</sup> duration of 484.5 ms [30 frames]) scaled to maintain a constant number of effective (full contrast) cycles within the window.<sup>24</sup>

#### **Psychophysical Procedure**

Thresholds for area and luminance-modulated achromatic spot stimuli were measured with a 1/1 staircase randomly interleaved by location and yes/no response paradigm terminating after six reversals, with the threshold taken as the mean of the final four reversals. For AMS, area changed by 20% up to the first reversal in the staircase, then by 10% up to the second reversal, and 5% thereafter. For luminance modulated stimuli, contrast changed by 0.5 log units (5 dB) up to the first reversal, 0.25 log units (2.5 dB) up to the second reversal, 0.1 log units (1 dB) up to the third reversal, and 0.05 log units (0.5 dB) thereafter. For both area and luminance-modulated stimuli, a listening window of 2 seconds was permitted after stimulus offset in all trials, with the stimulus assumed to be unseen if no response was collected within this period. Falsepositive responses were tested for with zero contrast presentations ( $\sim 20\%$  of total presentations), with data for a given test excluded and repeated if the falsepositive rate exceeded 20%.

PGRA thresholds were measured with a twoalternative forced choice procedure and randomly interleaved by location three-up/one-down staircase terminating after four reversals, with the threshold taken as the mean of all reversals. Participants were required to press one of two buttons to indicate whether the gratings presented were orientated vertically (90°) or horizontally (180°). Vertical and horizontal grating orientations (90° and 180°) were selected given that test locations were along oblique meridians, to ensure both orientations were equally resolvable and prevent bias owing to orientation cues.<sup>23,24</sup> Stimulus spatial frequency changed by 20% until the first reversal, 10% until the second reversal, and 5% thereafter.

Before experiments with area-modulated, luminance-modulated, and PGRA stimuli, a practice run was provided to each observer, with study measurements commencing only when it was clear that the participant fully understood the test.

## **Energy Thresholds**

Area and contrast thresholds were converted to common energy units (E, cd/m<sup>2</sup>.s.deg<sup>2</sup>) as the product of increment luminance (cd/m<sup>2</sup>), presentation duration

(s) and stimulus area (deg²) at threshold. If stimulus area in the area modulation test exceeded 50.27 deg² (diameter of 6°) or the luminance at threshold for luminance-modulation tests exceeded the maximum luminance output of the display monitor (121.1 cd/m²), data from that location were excluded from further analysis. Each observer's difference in energy threshold (log  $\Delta E$  [log cd/m².s.deg²]) between test locations (3°–10° eccentricity) was calculated for each stimulus (AMS, GIII, and GV).

#### **Colocalized RGCD Estimates**

Colocalized RGCD estimates (cells/mm<sup>2</sup>) were calculated using two independent methods using OCT measures (structural method) and PGRA measures (functional method).

#### Structural OCT Method

This method used individual OCT RGC layer (RGCL) thickness values, extracted over a 24° × 24° area from a 30° × 25° macular cube scan centered on the fovea (Spectralis OCT, Heidelberg Engineering). Mean corneal curvature values (Shin Nippon NVision-K 5001 binocular open-field autorefractor, Shin-Nippon) were input for each participant before scan capture to minimize the effects of interindividual variations in ocular magnification.<sup>25</sup> Each individual B-scan was also examined by a trained observer, with any automated segmentation errors being manually corrected as necessary. An 8 × 8 grid, with each square measuring 3° × 3°, was centered over the fovea. The mean RGCL thickness was extracted from the grid squares corresponding with the visual field test locations, after correcting for RGC displacement from underlying photoreceptors. 26,27 RGCD was subsequently calculated using the methodology originally described by Raza and Hood<sup>28</sup> and the model of Drasdo et al.,<sup>26</sup> incorporating the adjustments of Montesano et al.<sup>27</sup> For all calculations, the abbreviated AL method of Bennett et al.<sup>29</sup> was used to produce a conversion factor (qp) to translate degrees in visual space to mm on the retina. Briefly, this required the conversion factor (q) to be calculated for the fovea (q0 = 0.01306\*[AL - 1.82]), with an alteration being made for the eccentricity (U, in degrees) at which the functional measures were performed (qp = q0-0.000014U<sup>2</sup>). The theoretical basis of this model is an average three-surface (Bennett–Rabbetts) schematic eye that assumes the distance between the anterior corneal surface to the first principal point to be 1.82 mm, with the only free parameter being AL (in millimeters). Using qp, the eccentricity and stimulus diameter were converted to millimeters on the retina. In the current study, where Knapp's law was invoked and interobserver retinal image size was constant in millimeters on the retina, an AL value equal to that expected in an emmetropic eye (23.3 mm) was used for the calculation of qp.

RGCD values at each test location were extracted in a two-step process. The first step involved calculating the number of RGC receptive fields underlying a GIII stimulus (0.14 deg<sup>2</sup>) for each participant using the normative, histological RGC counts for an age-similar cohort<sup>14</sup> and scaling to simulate a simple global expansion (balloon) model of myopia. To do this, normative histological RGC counts (RGC/mm<sup>2</sup>) from four primary meridians reported by Curcio and Allen<sup>14,30</sup> were linearly interpolated along polar coordinates. This generated estimates of RGC/mm<sup>2</sup> at 10,000 locations across the central retina, with the fovea and optic nerve aligned with the horizontal (0°) meridian. This interpolated RGC/mm<sup>2</sup> map was then rotated to align with each individual's OCT-measured fovea-disc angle and scaled according to the degree to which each observer's AL varied from the mean of the histological samples used  $^{14,30}$  (scaling factor = 23.84/AL). This calculation assumes a global expansion model of myopia in which RGC number remains constant as RGCD uniformly and proportionally changes with axial elongation. 12,27,31 The RGCD under the area of a GIII stimulus was established at the retinal position corresponding to visual field test locations. The retinal position (in millimeters) and area (in square millimeters) of the stimulus were determined using the conversion factor qp and adjusted for the lateral RGC displacement from underlying photoreceptors and individual AL.<sup>26,27</sup> To minimize error in this step, both the location of the stimulus centre and circumference were adjusted for the displacement from underlying photoreceptors and individual AL.<sup>27,32</sup> Although this correction was important to minimize error at both locations considered in this study, the magnitude of this correction was greatest for the 3° location.<sup>27</sup>

In the second step, pointwise RGC/mm<sup>2</sup> data (from step 1) were converted to volumetric density (RGC/mm<sup>3</sup>) by dividing by the average RGCL thickness (millimeters) in the corresponding OCT grid square (3° × 3°) measured for the full cohort, using a leave-one-out technique.<sup>28</sup> Volumetric density values were subsequently convolved with colocalized RGCL thickness (millimeters) measures for each individual to produce localized RGCD (cells/mm<sup>2</sup>) measures. This analysis was repeated for each visual field location with the retinal position (in millimeters) of the stimulus (and thus corresponding OCT grid square) deter-

mined using the conversion factor qp and adjusted for the lateral displacement of RGCs from underlying photoreceptors and individual AL.<sup>26,27</sup>

#### **Functional PGRA Method**

This method determined functional RGCD estimates from PGRA measures. Here PGRA thresholds were converted to minimum angle of resolution values and subsequently RGCD using the equation<sup>33</sup> minimum angle of resolution =  $0.93/\sqrt{D}$ , where D = RGC/deg<sup>2</sup>. Similar to the OCT method, a conversion factor for individual test locations (qp) was used to translate visual angle to retinal eccentricity (mm).

For both structural (OCT-derived RGCD [RGCD<sub>OCT</sub>]) and functional (PGRA-derived RCGD [RGCD<sub>PGRA</sub>]) methods, the absolute difference in RGCD measures (log  $|\Delta$ RGCD| [log cells/mm<sup>2</sup>]) between test locations (3°–10° eccentricity) was then calculated for each observer.

## Structure–Function and Function–Function Ratios

Ratios of  $\Delta E/|\Delta RGCD|$  were calculated for each participant as the quotient of their respective log  $\Delta E$ and log |RGCD| gradient values. Eccentricity differences in AMS, GIII, and GV thresholds were each taken as measures of  $\Delta E$ . Eccentricity differences in RCGD, separately for RGCD<sub>OCT</sub> and RGCD<sub>PGRA</sub> methods were taken as measures of the  $\triangle$ RGCD. An important assumption in this study is that a ratio of 1 would indicate the structural and functional measures with the greatest concordance (i.e., a 1:1 relationship). In other words, this ratio would indicate that eccentricity-related changes in threshold with the stimulus in question varied directly proportionally with eccentricity-related changes in RGCD. This methodology was designed to relate physiological changes in functional thresholds and in vivo RGCD estimates on a colocalized and individualized basis, to minimize the impact of interindividual differences in both structure and function. 15,34

## **Statistical Analysis**

Friedman tests with post hoc Wilcoxon signed rank tests (where indicated) were used to test for statistically significant differences in energy threshold gradients (log  $\Delta E$ ) and  $\Delta E/|\Delta RGCD|$  ratio values between stimuli, as well as statistically significant differences in RGCD (log cells/mm²) between eccentricities and estimation methods. Mann–Whitney U tests

were used to test for statistically significant differences in energy thresholds, RGCD, and  $\Delta E/|\Delta RGCD|$  ratio values between the myopic and nonmyopic subgroups. Statistical analyses were carried out in MATLAB (2023b, The MathWorks, Natick, MA), where alpha = 0.05 was considered statistically significant. P values were adjusted using Holm–Bonferroni correction where multiple tests of the same hypothesis were undertaken.

## **Results**

#### **Function: Energy Thresholds**

Statistically significant differences in energy thresholds between 3° and 10° (log  $\Delta E$ ) were observed for the three stimulus forms examined, Friedman test:  $\chi^2$  (2) = 67.22, P < 0.001. These energy differences were largest for AMS (median, 0.30; IQR, 0.20–0.46), followed by GIII (median, 0.16; IQR, 0.04–0.23) and smallest for GV (median, 0.08; IQR, 0.01–0.16). Post hoc tests also revealed statistically significant differences between each individual stimulus pair (AMS vs GIII and GV, both P < 0.001; GIII vs GV, P < 0.01) (Fig. 1). For all stimuli and test locations, no statistically significant differences in energy thresholds (log E) were found between myopes (all myopes or high myopes only) and nonmyopes (Table 2).

#### **Structure: Colocalized RGCD Estimates**

RGCD (log cells/mm<sup>2</sup>) was statistically significantly higher at 3° compared with 10° for measures derived from both structural (OCT) and functional (PGRA) methods (3°, OCT median, 4.36 [IQR, 4.31-4.42]; PGRA median, 3.30 [IQR, 3.14–3.52]; 10°, OCT median, 3.83 [IQR, 3.75-3.87]; PGRA median, 2.89 [IQR, 2.77–3.01]) (Wilcoxon signed-rank test, both P < 0.001) (Fig. 2). RGCD estimates and log  $|\Delta$ RGCD gradients were statistically significantly greater with the OCT method compared with the PGRA method (Wilcoxon signed-rank test, all P < 0.001). Furthermore, RGCD measures were statistically significantly lower in the myopic group compared with the nonmyopic control group at both locations examined when using OCT-derived RGCD measures (Mann-Whitney U test, both P < 0.001); however, these differences failed to reach statistical significance for PGRAderived RGCD estimates (3°, P = 0.37; 10°, P = 0.14).

## Structure–Function and Function–Function Ratios

 $\Delta E/|\Delta RGCD_{OCT}|$  ratio values were 0.54 (IQR, 0.37–0.78) for AMS, 0.29 (IQR, 0.08–0.44) for GIII, and 0.16 (IQR, 0.02–0.29) for GV (Fig. 3a). Following the same trend, the  $\Delta E/|\Delta RGCD_{PGRA}|$  ratio values were 0.71 (IQR, 0.46–1.19) for AMS, 0.33 (IQR,

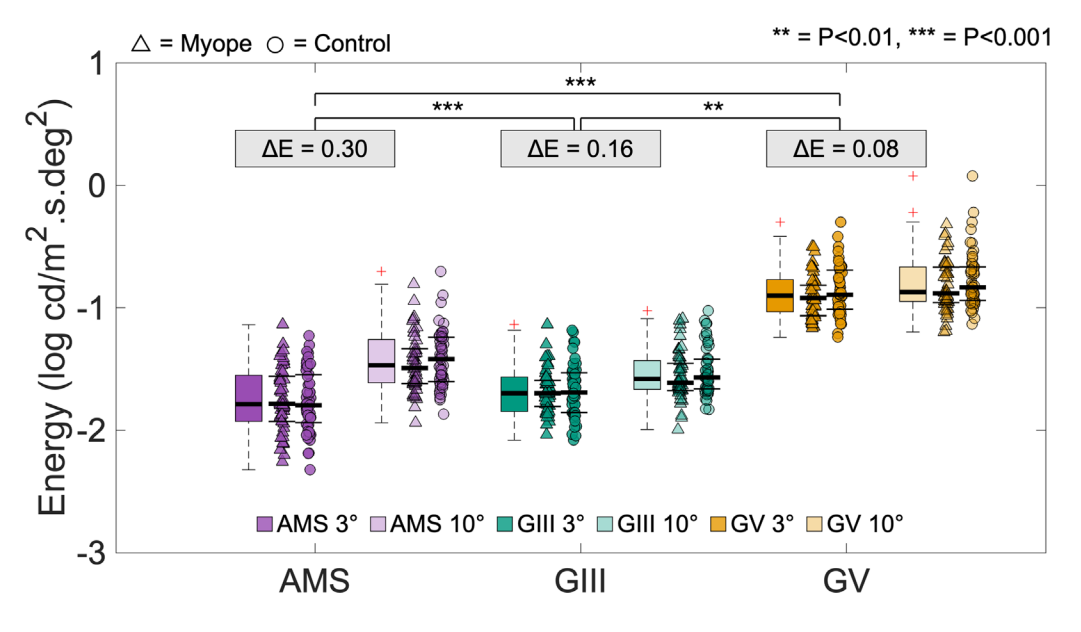
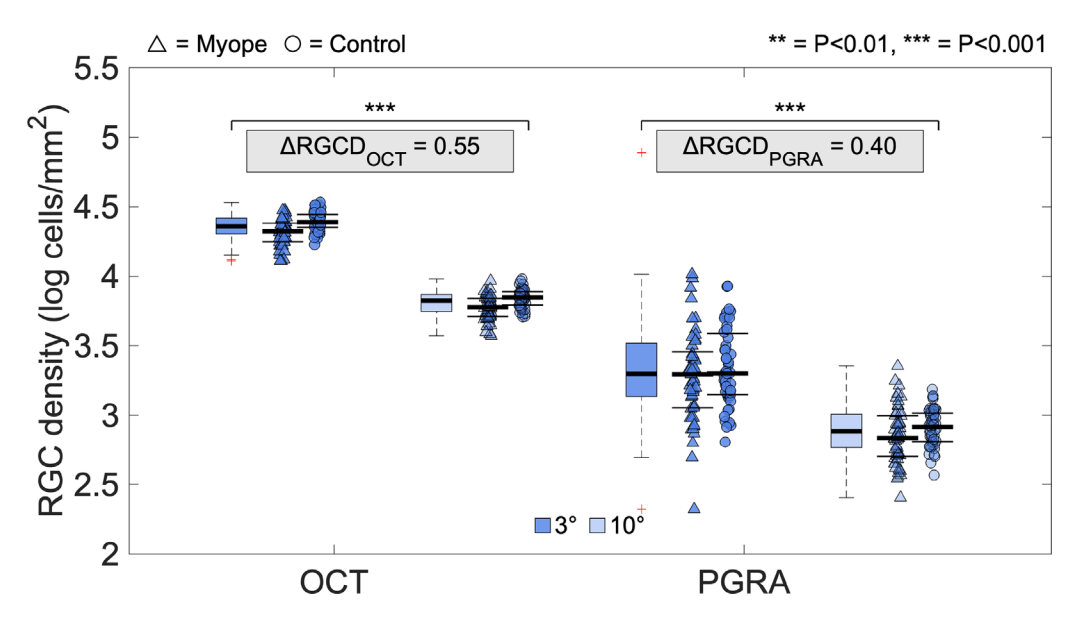


Figure 1. Energy thresholds for AMS, GIII, and GV stimuli at 3° and 10° eccentricity. Individual data points are included as triangle markers (myopic observers) and spot markers (nonmyopic observers), with median (bold line) and 25th and 75th percentiles (fine lines) also included for reference. The median log difference in energy thresholds between 3° and 10° eccentricity for each stimulus ( $\Delta E$ ) across all participants is displayed in the corresponding gray box.

Table 2. Energy Thresholds (log cd/m<sup>2</sup>.s.deg<sup>2</sup>) at 3° and 10° Eccentricity

		Myopes		P Value	
	Nonmyopes (A) $(n = 51)$	All Myopes (B) $(n = 49)$	High Myopes (C) $(n = 11)$	A vs. B	A vs. C
AMS					
3°	-1.80	<b>-1.78</b>	<b>–1.59</b>	0.73	0.06
	[-1.55 to -1.94]	[-1.56 to -1.93]	[-1.40  to  -1.79]		
10°	-1.42	<b>—1.49</b>	-1.40	0.73	0.81
	[-1.24 to -1.60]	[-1.33 to -1.62]	[-1.34  to  -1.55]		
GIII					
3°	<b>–1.69</b>	<b>-1.70</b>	-1.62	0.67	1.32
	[-1.53 to -1.86]	[-1.59 to -1.81]	[-1.60  to  -1.71]		
10°	<b>–1.57</b>	-1.61	<b>–1.58</b>	0.88	1.32
	[-1.42 to -1.66]	[-1.45 to -1.68]	[-1.50 to -1.65]		
GV					
3°	-0.89	-0.92	-0.92	0.33	0.60
	[-0.69 to -1.01]	[-0.82 to -1.06]	[-0.90  to  -0.98]		
10°	-0.83	-0.88	-0.87	0.33	0.60
	[-0.67  to  -0.94]	[-0.67  to  -0.96]	[-0.69 to -0.93]		

High myopes are defined as having a mean spherical equivalent of  $\leq$  -6.00 D. Values are median [IQR]. *P* values were calculated using the Mann–Whitney *U* test and have been adjusted for multiple comparisons using Holm–Bonferroni correction.



**Figure 2.** Boxplots of RGCD estimates for OCT and PGRA methods at 3° and 10° eccentricity. *Triangle markers* represent data from myopic observers and spot markers represent data from nonmyopic observers. Median and 25th and 75th percentiles are included as *bold* and *fine lines*, respectively for each dataset. The median log change in RGCD between 3° and 10° eccentricity for each method across all participants is displayed in the corresponding *gray box*.

0.07–0.54) for GIII, and 0.19 (IQR, 0.02–0.44) for GV (Fig. 3b). For both RGCD estimation methods, interstimulus differences in ratio values were statistically significant, RGCD<sub>OCT</sub>, Friedman test,  $\chi^2$  (2) = 67.22,  $P \le 0.001$ ; RCGD<sub>PGRA</sub>,  $\chi^2$  (2) = 67.22,

 $P \le 0.001$ , with post hoc Wilcoxon signed-rank tests revealing statistically significant differences between all stimulus pairs (AMS vs GIII, both P < 0.001; AMS vs GV, both P < 0.001; GIII vs GV, P < 0.01 for RGCD<sub>OCT</sub> and P = 0.03 for RCGD<sub>PGRA</sub>). The

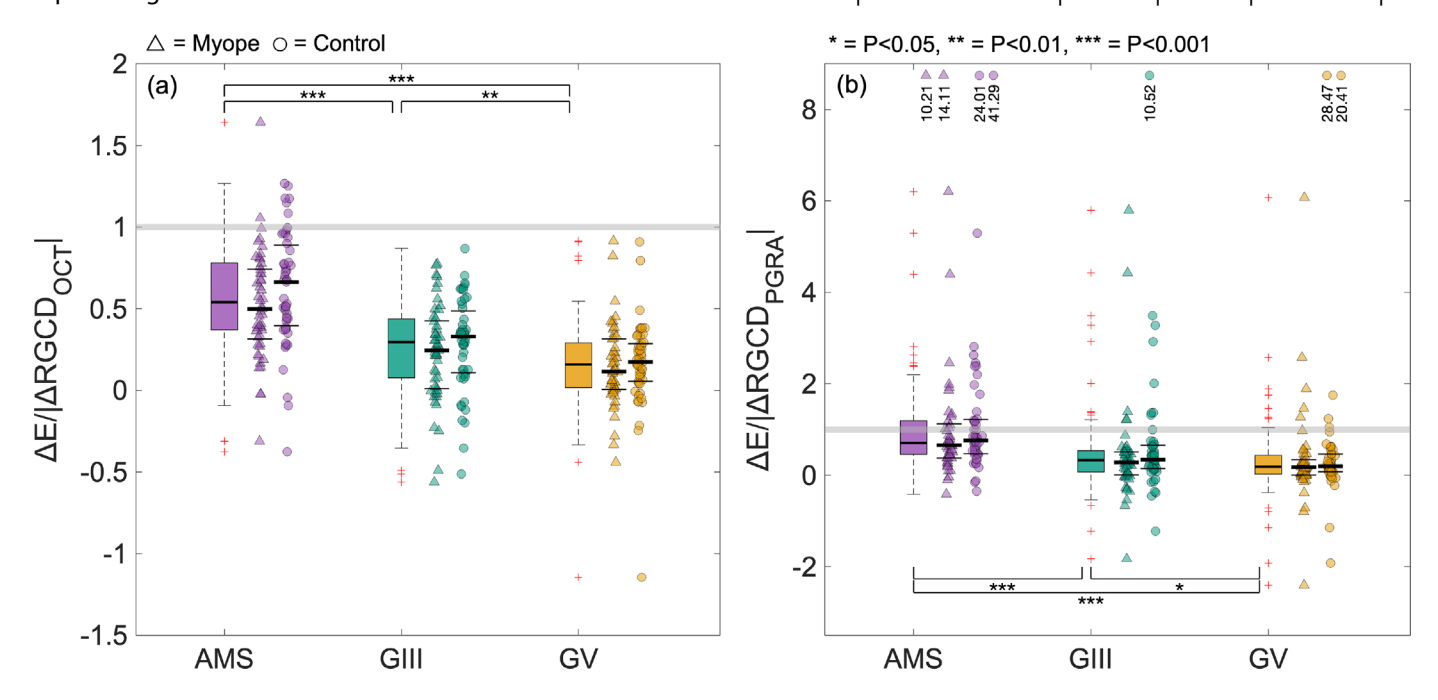


Figure 3.  $\Delta E/|\Delta RGCD|$  values for each stimulus using (a) OCT-informed and (b) PGRA-informed RGCD estimates. *Triangle markers* represent data from myopic observers and *spot markers* represent data from nonmyopic observers. Median and IQR (*bold and fine lines*, respectively) ratio values for each stimulus within the myopic and nonmyopic subgroups are displayed by the *black lines* on top of the corresponding data points. The *solid gray line* represents a 1:1 relationship between functional and structural gradients over the eccentricities tested (i.e.,  $\Delta E/|\Delta RGCD| = 1$ ). Extreme outlier data points in (b) are displayed at the top of the plot above a *y* axis break with their corresponding ratio value.

same trends were observed when analyzing the myopic  $(\Delta E/|\Delta RGCD_{OCT}|, AMS 0.50 [IQR, 0.31-0.74]; GIII$ 0.24 [IQR, 0.01–0.43]; GV 0.11 [IQR, 0.00–0.31];  $\Delta E/\Delta RGCD_{PGRA}$ , AMS 0.66 [IQR, 0.38–1.12]; GIII 0.28 [IQR, 0.01–0.51]; GV 0.18 [IQR, 0.00–0.34]) and nonmyopic (ΔΕ/|ΔRGCD<sub>OCT</sub>|, AMS 0.66 [IQR, 0.40– 0.89]; GIII 0.33 [IQR, 0.11-0.49]; GV 0.17 [IQR, 0.06-0.28];  $\Delta E/|\Delta RGCD_{PGRA}|$ , AMS 0.76 [IQR, 0.47-1.22]; GIII 0.34 [IQR, 0.15–0.66]; GV 0.20 [IQR, 0.08– 0.46] subgroups separately, with statistically significant differences between all stimulus pairs remaining in both subgroups (AMS vs GIII, both P < 0.001; AMS vs GV, both P < 0.001; GIII vs GV, P < 0.05for RGCD<sub>OCT</sub>) with the exception of GIII vs GV for RCGD<sub>PGRA</sub> in myopes (P = 0.41). No statistically significant differences in the  $\Delta E/|\Delta RGCD|$  ratio values were found for any stimuli when comparing the myopic and nonmyopic groups, (Mann–Whitney U test, RGCD<sub>OCT</sub>, all P > 0.27; RGCD<sub>PGRA</sub>, all P> 0.64). For all stimuli, ratio values calculated using RCGD<sub>PGRA</sub> estimates were higher than those that used RCGD<sub>OCT</sub> estimates, Friedman test,  $\chi^2$  (5) =134.91, P < 0.001. Post hoc tests only found statistically significant differences in ratio values between RCGD estimation methods for AMS and GV stimuli (Mann-Whitney U test, AMS, P < 0.001; GIII, P = 0.22; GV, P = 0.01).

### **Discussion**

In this study, we found greater eccentricity-related differences in threshold in healthy observers with an AMS designed to measure alterations in spatial summation, than with conventional, fixed-area SAP stimuli (GIII and GV) modulating in luminance. Furthermore, those eccentricity-related threshold differences with AMS showed a more directly proportional relationship with physiological variations in RGCD across the same area of the retina than did thresholds measured with conventional, luminance-modulated stimuli.

## **Ability to Detect RGCD Gradients**

In agreement with previous work that found a small glaucoma disease signal (log difference in energy thresholds [log  $\Delta E$ ] between glaucoma participants and healthy controls) using the GIII stimulus, <sup>7,10,13</sup> we found the sensitivity to physiological gradients in RGCD with eccentricity to be small for SAP stimuli (Fig. 1). In line with our stated hypothesis, we found that AMS thresholds, designed to measure changes in RA, better related to physiological gradients in RGCD, supporting previous studies displaying their

improved sensitivity to pathological deficits in RGCD in glaucoma. 6,7,9,10,13,35–37

Although such trends were in line with the previous literature, our finding of no statistically significant difference in AMS thresholds between myopic and nonmyopic subgroups was not in agreement with previous work.<sup>12</sup> Specifically, RA has been shown by Stapley et al.<sup>12</sup> (2020) to enlarge in spectaclecorrected axial myopes relative to nonmyopes in the absence of disease where Knapp's law was satisfied (to maintain a constant retinal image size in millimeters). We hypothesized that similar trends would be uncovered using AMS in this study where refractive error was corrected in an identical manner. One explanation for this discrepancy may relate to differences in participant characteristics, in particular the relatively small sample (n = 11) of high myopes in our current cohort. This subgroup had larger AMS thresholds relative to control and low/moderate myopic groups, although this difference failed to attain statistical significance (Table 2). There may also be differences in the proportion of axially myopic to nonaxially myopic participants between studies, as well as interindividual variations in the degree of retinal stretching, proposed to cause functional and/or structural differences between myopes and nonmyopes.<sup>31</sup> Methodological differences should also be considered. Stapley et al. 12 identified alterations in RA in axial myopia by measuring contrast thresholds for a range of stimuli of different area, which were then fitted with a statistical model to generate RA estimates. In this study, we measured AMS thresholds with a fixed luminance, selected based on the expected contrast threshold for a RA-scaled stimulus in observers aged 20 to 77 years, with refractive errors of less than  $\pm 6.00$  DS.<sup>7,11,35</sup> Future work is necessary to investigate the impact of age and AL on contrast thresholds at RA (these being factors shown to potentially alter the luminance expected at threshold for a RA-scaled stimulus<sup>12,21</sup>), and how this may influence the accuracy of AMS estimates of RA. Such information would be valuable to identify whether a constant stimulus luminance based on population averages may be applied for AMS, or whether this should be varied according to individual characteristics.

## RGCD Estimates Based on Structural and Functional Measures

In the absence of ground-truth RGC counts within our cohort, we estimated RGCD using two different methods, one using OCT RGCL thickness and the other using high-contrast PGRA thresholds. In line with the previous literature, our PGRA-derived RGCD estimates were markedly lower than OCTderived estimates.<sup>15</sup> It is hypothesized that the PGRA method samples only functionally active ON-midget RGCs, 15,38,39 whereas OCT measures include all neural and non-neural components of the RGCL (including all RGC subtypes, displaced amacrine cells, and other non-neural tissues). These differences may account for the higher  $\Delta E/|\Delta RGCD|$  ratios using PGRA compared with OCT estimates of RGCD, where the same log  $\Delta E$  for each stimulus was divided by a smaller log  $|\Delta RGCD|$ , leading to a higher ratio value. Another explanation might be that comparing a functional measure (log  $\Delta E$ ) to a structural metric derived from functional (PGRA) measures could result in a more proportional relationship (compared with the use of a true structural metric in the OCT method).

Although both methods have limitations, discussed in detail by Stapley et al., 15 they possess important advantages. Compared with a more generalized empirical approach, <sup>26,40,41</sup> both methods enabled the generation of personalized RGCD estimates for each participant by incorporating colocalized structural (OCT RGCL thickness) or functional (PGRA thresholds) data. The PGRA method in particular does not necessitate the use of normative histological RGC counts, these being available for only a small number of cadaver eyes with large intereye variations in RGCD  $(\sim 2\times$  at  $\sim 10^{\circ 14,30})$ . Furthermore, this method does not require assumptions around the nature of axial stretch in myopic observers or the colocalization of structural and functional (AMS and SAP) measures to be made. 15 Conversely, the OCT model is more objective, avoiding reliance on participant attention and responses, minimizing measurement error and variability,<sup>4,28</sup> which could confound psychophysical estimates. 15 A strength of our study is that structure function relationships calculated using both RGCD estimation methods display the same result, adding weight to the conclusion that AMS displays a more directly proportional relationship with RGCD in our cohort.

In line with previous reports of reduced RGCD in myopia, <sup>16,17,31</sup> we found a lower RGCD in the myopic group when using OCT-derived RGCD estimates. However, this finding did not hold true for PGRA-derived estimates, in contrast with a recent study applying the same method in a myopic cohort. <sup>15</sup> A potential explanation is that, particularly at the more central 3° test location, resolution may have been optically limited in some individuals, particularly in observers with a greater AL, for whom (according to Knapp's law<sup>19</sup>) the stimulus may fall at an angular (degrees) eccentricity closer to the fovea (constant

across all observers in millimeters). This could impact upon the relative accuracy of PGRA-derived RGCD measures at this location, a fundamental assumption of which is that resolution acuity is neurally (and not optically) limited. <sup>17,33,39,42,43</sup> Although previous work by Green<sup>44</sup> and Chui et al. <sup>17</sup> suggests resolution to be neurally limited at 3°, participant characteristics may not directly correspond between studies; hence, it remains important to consider optical effects as a potential confounder.

# Structure-Function and Function-Function Relationships

Our finding of a shallow and variable structurefunction relationship for fixed area stimuli (GIII<sup>3,4,6,45</sup> and GV<sup>46</sup>) is in line with previous studies in both glaucomatous<sup>45,47</sup> and healthy<sup>2,3,6</sup> eyes. Such findings have been attributed, at least in part, to the fact that these fixed-area stimuli do not directly account for differences in spatial summation that occur with both physiological (e.g., with retinal/visual field eccentricity<sup>11</sup>) and pathological (e.g., in glaucoma<sup>7</sup>) changes in RGCD. Swanson et al.<sup>3</sup> reported that, in a healthy observer, the relationship between GIII thresholds (in decibels) and log RGC counts underlying these stimuli (derived from histological counts<sup>14</sup>) could be well-described by a two-line model in which a slope of 1 (i.e., 1:1 relationship) described the relationship for visual field locations of more than approximately 15°, this slope flattening for more central locations. Similar relationships have been reported in other work in both primate<sup>4</sup> and human observers,<sup>2,48</sup> proposed to relate to the enlargement of RA with eccentricity<sup>11</sup> to maintain input from a constant number of RGCs to cortical receptive fields.<sup>7,40</sup> Redmond et al.<sup>7</sup> also found a reduction in PGRA-derived RGCD to accompany an increase in RA in participants with and without glaucoma, this being the first prospective study to suggest that RA encompasses input from a constant number of RGCs in glaucoma. Later, Yoshioka et al.<sup>6</sup> found the relationship between contrast thresholds and colocalized OCT-derived RGC number to approach 1:1 for a GI stimulus within the central 10°, this relationship becoming shallower (i.e., a >1 log-unit change in structure was needed to yield a 1 log-unit change in threshold) for larger stimuli in both control and glaucoma observers. Our finding of structure-function and function-function relationships that approach 1:1 for AMS, specifically designed to self-scale to the localized RA at threshold, supports the hypothesis that such stimuli directly target a parent functional biomarker (changes in RA), whereas luminance-modulated stimuli only indirectly target it by measuring the secondary consequences of an altered RA.

Although the structure–function and function– function relationships for AMS found in this study approached 1:1, they did not reach exact reciprocity (1:1 ratio) as hypothesized. There are a number of factors that may explain this. The first may relate to variability of both functional and structural measures. which may also account for the range of ratio values found for all stimuli, particularly when using functional PGRA-derived RCGD estimates (Fig. 3b). Although possible, recent research by Rountree et al. 13 found response variability to be more uniform with depth of defect with AMS than with GIII, suggesting that a structure-function relationship approaching 1:1 should be more consistently observed with AMS. 13 Other potential explanatory factors are differences in the population of RGCs responding to the psychophysical stimuli compared with that sampled by the RGCD estimation methods used, and how their distribution alters with eccentricity. Specifically, previous work suggests magnocellular (parasol) RGCs are most responsive to short duration achromatic perimetric stimuli (e.g., GIII<sup>49</sup>), whereas parvocellular (midget) RGCs are hypothesized to moderate resolution acuity tasks for high contrast gratings, 15,39,49 and all (neural and non-neural) components of the RGCL are included in the OCT model. Further, the ratios of midget-to-parasol and ON-to-OFF RGCs vary with increasing retinal eccentricity, whereby the proportion of midget cells decline, and both parasol cells and OFF-cell subtypes increase.<sup>38</sup> Across eccentricities examined in this study (3°-10°), these shifts are expected to be small, and in the absence of consensus on which RGC subtypes primarily mediate perimetric responses, the implications of these changes on measured ratios are difficult to anticipate, but important to consider.<sup>38</sup> Another important consideration is that the hypothesized 1:1 structure-function relationship with stimuli that undergo complete spatial summation at threshold is based on the assumption that a constant number of RGCs underlie RA (and therefore AMS thresholds).<sup>7,40</sup> However, previous work by Kwon and Lui<sup>40</sup> and Montesano et al.<sup>50</sup> both appear to find a departure from a constant number of RGCs underlying RA between the central and peripheral visual field  $(4.0^{\circ}-8.5^{\circ40})$  and  $1.4^{\circ}-9.9^{\circ50}$ , where a greater number of RGCs are found to underlie RA at smaller eccentricities. Montesano et al. <sup>50</sup> proposed this to relate to changes in cone-RGC convergence with retinal eccentricity. Accordingly, if RGC number underlying RA does indeed vary between test locations in this study (3°–10°), this may have contributed to our finding of a structure–function and function–function ratio of less than 1:1 for AMS.

Previous studies have indicated that RGCL thickness, RGCD, and perimetric sensitivity vary with age<sup>21,51-53</sup> and axial myopia. 54-60 These are potential confounders when examining the structure-function relationship in healthy and diseased cohorts. An advantage of our methodology using ratios of the log change in energy thresholds and RGCD with eccentricity on a per-participant basis is that these differences are accounted for within each individual. To date, this methodology has not been applied in participants with glaucoma, in whom variations in RGCD are pathological rather than physiological. However, on the basis of previous work<sup>2,3,6,7</sup> it could be hypothesized that a ratio approximating 1:1 would also be observed where a stimulus undergoing complete spatial summation at threshold is used (AMS).

#### Translational Relevance of This Work

We found AMS to display a more directly proporstructure-function and function-function relationship with underlying RGCD in healthy observers (i.e.,  $\Delta E/|\Delta RGCD|$  ratio value closest to 1), compared with conventional SAP stimuli of fixed area (GIII and GV), modulating in luminance. This finding was present in both nonmyopic and myopic observers, in whom RGCD and RA alter in the absence of glaucoma. 12 This work supports the notion that accounting for physiological changes to spatial summation with eccentricity<sup>11</sup> strengthens the structure-function relationship in both myopic and nonmyopic eyes.<sup>3,6</sup> Given that changes in RA in glaucoma are similar to those observed with retinal eccentricity in healthy eyes, our findings, like previous work, <sup>7,34,6,9,10,13,35,61,62</sup> suggest AMS holds promise to improve the detection and monitoring of functional loss associated with RGCD changes in glaucoma with perimetry.

## Acknowledgments

Supported by a PhD studentship from the Department for the Economy, Northern Ireland (CSC). and in part by the National Institute for Health and Care Research (NIHR) Biomedical Research Centre based at Moorfields Eye Hospital NHS Foundation Trust and UCL Institute of Ophthalmology (PJM, DFG-H, and RSA). DFG-H's chair at UCL is supported by funding from Glaucoma UK. The views expressed are those of

the authors and not necessarily those of the NHS, the NIHR, or the Department of Health.

**Author Contributions:** Study concept and design: P.J.M., R.S.A., V.S., T.R., C.S.C., D.F.G.-H.; Acquisition of data: C.S.C.; Analysis and interpretation of data: C.S.C., V.S., P.J.M., R.S.A., T.R.; Drafting of the manuscript: C.S.C.; Critical review of the manuscript: All authors.

**Data Availability:** Supporting data will be made available upon request from the corresponding author.

Disclosure: C.S. Campbell, None; V. Stapley, LKC Inc (R); R.S. Anderson, Alliance Pharmaceuticals Ltd (R), Moorfields Acuity Chart (O), Visual Field Sensitivity Testing (P); D.F. Garway-Heath, Visual Field Sensitivity Testing (P), T4 (P), Alcon Research Institute (F), Janssen (F, C), Santen (F, C), CenterVue (R, C), Oculus (R), Topcon (R), Abbvie (C), Omikron (C), CREWT Medical Systems Inc. (F); T. Redmond, Visual field sensitivity testing (P), Heidelberg Engineering GmbH (F), CREWT Medical Systems Inc. (F); P.J. Mulholland, Visual field sensitivity testing (P), Heidelberg Engineering Gmbh (F), LKC Inc. (F), CREWT Medical Systems Inc. (F)

### References

- 1. Camp AS, Weinreb RN. Will perimetry be performed to monitor glaucoma in 2025? *Ophthalmology*. 2017;124:S71–S75.
- 2. Garway-Heath DF, Caprioli J, Fitzke FW, Hitchings RA. Scaling the hill of vision: the physiological relationship between light sensitivity and ganglion cell numbers. *Invest Ophthalmol Vis Sci.* 2000;41:1774–1782.
- 3. Swanson WH, Felius J, Pan F. Perimetric defects and ganglion cell damage: interpreting linear relations using a two-stage neural model. *Invest Ophthalmol Vis Sci.* 2004;45:466.
- 4. Harwerth RS, Carter-Dawson L, Smith EL, Barnes G, Holt WF, Crawford MLJ. Neural losses correlated with visual losses in clinical perimetry. *Invest Ophthalmol Vis Sci.* 2004;45:3152.
- 5. Harwerth RS, Quigley HA. Visual field defects and retinal ganglion cell losses in patients with glaucoma. *Arch Ophthalmol*. 2006;124:853–859.
- 6. Yoshioka N, Zangerl B, Phu J, et al. Consistency of structure-function correlation between spatially scaled visual field stimuli and in vivo OCT ganglion cell counts. *Invest Ophthalmol Vis Sci.* 2018;59:1693.

- 7. Redmond T, Garway-Heath DF, Zlatkova MB, Anderson RS. Sensitivity loss in early glaucoma can be mapped to an enlargement of the area of complete spatial summation. *Invest Ophthalmol Vis Sci.* 2010;51:6540.
- 8. Zalta AH, Burchfield JC. Detecting early glaucomatous field defects with the size I stimulus and Statpac. *Br J Ophthalmol*. 1990;74: 289.
- 9. Kalloniatis M, Khuu SK. Equating spatial summation in visual field testing reveals greater loss in optic nerve disease. *Ophthalmic Physiol Opt.* 2016;36:439–452.
- 10. Mulholland PJ, Redmond T, Garway-Heath DF, Zlatkova MB, Anderson RS. Spatiotemporal summation of perimetric stimuli in early glaucoma. *Invest Ophthalmol Vis Sci.* 2015;56:6473.
- 11. Wilson ME. Invariant features of spatial summation with changing locus in the visual field. *J Physiol*. 1970;207:611–622.
- 12. Stapley V, Anderson RS, Saunders KJ, Mulholland PJ. Altered spatial summation optimizes visual function in axial myopia. *Sci Rep.* 2020;10:12179.
- 13. Rountree L, Mulholland PJ, Anderson RS, Garway-Heath DF, Morgan JE, Redmond T. Optimising the glaucoma signal/noise ratio by mapping changes in spatial summation with area-modulated perimetric stimuli. *Sci Rep.* 2018;8:2172.
- 14. Curcio CA, Allen KA. Topography of ganglion cells in human retina. *J Comp Neurol*. 1990;300:5–25.
- 15. Stapley V, Anderson RS, Saunders K, Mulholland PJ. Examining the concordance of retinal ganglion cell counts generated using measures of structure and function. *Ophthalmic Physiol Opt.* 2022;42:1338–1352.
- 16. Wolsley CJ, Saunders KJ, Silvestri G, Anderson RS. Investigation of changes in the myopic retina using multifocal electroretinograms, optical coherence tomography and peripheral resolution acuity. *Vis Res.* 2008;48:1554–1561.
- 17. Chui TYP, Yap MKH, Chan HHL, Thibos LN. Retinal stretching limits peripheral visual acuity in myopia. *Vis Res.* 2005;45:593–605.
- Flitcroft DI, He M, Jonas JB, et al. IMI defining and classifying myopia: a proposed set of standards for clinical and epidemiologic studies. *Invest Ophthalmol Vis Sci.* 2019;60:M20–M30.
- 19. Knapp H. The influence of spectacles on the optical constant and visual acuteness of the eye. *Arch Ophthalmol*. 1869;1:377–410.

- 20. Bridgeman B. Durations of stimuli displayed on video display terminals: (n 1)/f + persistence. *Psychol Sci.* 1998;9:232–233.
- 21. Redmond T, Zlatkova MB, Garway-Heath DF, Anderson RS. The effect of age on the area of complete spatial summation for chromatic and achromatic stimuli. *Invest Ophthalmol Vis Sci.* 2010;51:6533.
- 22. Stiles WS. Color vision: the approach through increment-threshold sensitivity. *Proc Natl Acad Sci USA*. 1959;45:100–114.
- 23. Rovamo J, Virsu V, Laurinen P, Hyvarinen L. Resolution of gratings oriented along and across meridians in peripheral vision. *Invest Ophthalmol Vis Sci.* 1982;23:666–670.
- 24. Anderson RS, McDowell DR. Peripheral resolution using stationary and flickering gratings: the effects of age. *Curr Eye Res.* 1997;16:1209–1214.
- 25. Ctori I, Gruppetta S, Huntjens B. The effects of ocular magnification on Spectralis spectral domain optical coherence tomography scan length. *Graefes Arch Clin Exp Ophthalmol*. 2015;253:733–738.
- 26. Drasdo N, Millican CL, Katholi CR, Curcio CA. The length of Henle fibers in the human retina and a model of ganglion receptive field density in the visual field. *Vis Res.* 2007;47:2901–2911.
- 27. Montesano G, Ometto G, Hogg RE, Rossetti LM, Garway-Heath DF, Crabb DP. Revisiting the Drasdo model: implications for structure-function analysis of the macular region. *Transl Vis Sci Technol*. 2020;9:15.
- 28. Raza AS, Hood DC. Evaluation of the structure–function relationship in glaucoma using a novel method for estimating the number of retinal ganglion cells in the human retina. *Invest Ophthalmol Vis Sci.* 2015;56:5548.
- 29. Bennett AG, Rudnicka AR, Edgar DF. Improvements on Littmann's method of determining the size of retinal features by fundus photography. *Graefes Arch Clin Exp Ophthalmol*. 1994;232:361–367.
- 30. Curcio CA, Sloan KR, Meyers D. Computer methods for sampling, reconstruction, display and analysis of retinal whole mounts. *Vis Res.* 1989;29:529–540.
- 31. Atchison DA, Jones CE, Schmid KL, et al. Eye shape in emmetropia and myopia. *Invest Ophthalmol Vis Sci.* 2004;45:3380.
- 32. Tong J, Phu J, Alonso-Caneiro D, Khuu SK, Kalloniatis M. Clinical evaluations of macular structure-function concordance with and without Drasdo displacement. *Transl Vis Sci Technol*. 2022;11:18.

- 33. Thibos LN, Cheney FE, Walsh DJ. Retinal limits to the detection and resolution of gratings. *J Opt Soc Am A*. 1987;4:1524.
- 34. Anderson RS. The psychophysics of glaucoma: improving the structure/function relationship. *Prog Retin Eye Res.* 2006;25:79–97.
- 35. Phu J, Khuu SK, Zangerl B, Kalloniatis M. A comparison of Goldmann III, V and spatially equated test stimuli in visual field testing: the importance of complete and partial spatial summation. *Ophthalmic Physiol Opt.* 2017;37:160–176.
- 36. Phu J, Khuu SK, Bui BV, Kalloniatis M. A method using Goldmann stimulus sizes I to V-measured sensitivities to predict lead time gained to visual field defect detection in early glaucoma. *Transl Vis Sci Technol*. 2018;7:17.
- 37. Phu J, Khuu SK, Nivison-Smith L, Kalloniatis M. Standard automated perimetry for glaucoma and diseases of the retina and visual pathways: current and future perspectives. *Prog Retin Eye Res.* 2025;104:101307.
- 38. Dacey DM. The mosaic of midget ganglion cells in the human retina. *J Neurosci*. 1993;13:5334–5355.
- 39. Anderson RS, Zlatkova MB, Demirel S. What limits detection and resolution of short-wavelength sinusoidal gratings across the retina? *Vis Res.* 2002;42:981–990.
- 40. Kwon M, Liu R. Linkage between retinal ganglion cell density and the nonuniform spatial integration across the visual field. *Proc Natl Acad Sci USA*. 2019;116:3827–3836.
- 41. Watson AB. A formula for human retinal ganglion cell receptive field density as a function of visual field location. *J Vis.* 2014;14:15.
- 42. Thibos LN. Acuity perimetry and the sampling theory of visual resolution. *Optom Vis Sci.* 1998;75:399–406.
- 43. Thibos LN, Walsh DJ, Cheney FE. Vision beyond the resolution limit: aliasing in the periphery. *Vis Res.* 1987;27:2193–2197.
- 44. Green DG. Regional variations in the visual acuity for interference fringes on the retina. *J Physiol*. 1970;207:351–356.
- 45. Quigley HA, Dunkelberger GR, Green WR. Retinal ganglion cell atrophy correlated with automated perimetry in human eyes with glaucoma. *Am J Ophthalmol*. 1989;107:453–464.
- 46. Yanagisawa M, Murata H, Matsuura M, Fujino Y, Hirasawa K, Asaoka R. Investigating the structure-function relationship using Goldmann V standard automated perimetry where glaucomatous damage is advanced. *Ophthalmic Physiol Opt.* 2019;39:441–450.

- 47. Harwerth RS, Carter-Dawson L, Shen F, Smith EL, Crawford ML. Ganglion cell losses underlying visual field defects from experimental glaucoma. *Invest Ophthalmol Vis Sci.* 1999;40:2242–2250.
- 48. Tribble JR, Vasalauskaite A, Redmond T, et al. Midget retinal ganglion cell dendritic and mitochondrial degeneration is an early feature of human glaucoma. *Brain Commun*. 2019;1:fcz035.
- 49. Swanson WH, Sun H, Lee BB, Cao D. Responses of primate retinal ganglion cells to perimetric stimuli. *Invest Ophthalmol Vis Sci.* 2011;52:764.
- 50. Montesano G, Mulholland PJ, Garway-Heath DF, Evans J, Ometto G, Crabb DP. Spatiotemporal summation of perimetric stimuli in healthy observers. *J Vis.* 2023;23:2.
- 51. Heijl A, Lindgren G, Olsson J. Normal variability of static perimetric threshold values across the central visual field. *Arch Ophthalmol*. 1987;105:1544–1549.
- 52. Phu J, Khuu SK, Nivison-Smith L, et al. Pattern recognition analysis reveals unique contrast sensitivity isocontours using static perimetry thresholds across the visual field. *Invest Ophthalmol Vis Sci.* 2017;58:4863–4876.
- 53. Demirkaya N, van Dijk HW, van Schuppen SM, et al. Effect of age on individual retinal layer thickness in normal eyes as measured with spectral-domain optical coherence tomography. *Invest Ophthalmol Vis Sci.* 2013;54:4934–4940.
- 54. Rudnicka AR, Edgar DF. Automated static perimetry in myopes with peripapillary crescents part I. *Ophthalmic Physiol Opt.* 1995;15:409–412.
- 55. Aung T, Foster PJ, Seah SK, et al. Automated static perimetry: the influence of myopia and its method of correction. *Ophthalmology*. 2001;108:290–295.
- 56. Lin F, Chen S, Song Y, et al. Classification of visual field abnormalities in highly myopic eyes without pathologic change. *Ophthalmology*. 2022;129:803–812.
- 57. Greve EL, Furuno F. Myopia and glaucoma. *Graefes Arch Klin Exp Ophthalmol*. 1980;213:33–41.
- 58. Jiang J, Song Y, Kong K, et al. Optic nerve head abnormalities in nonpathologic high myopia and the relationship with visual field. *Asia Pac J Ophthalmol*. 2023;12:460–467.
- 59. Seo S, Lee CE, Jeong JH, Park KH, Kim DM, Jeoung JW. Ganglion cell-inner plexiform layer and retinal nerve fiber layer thickness according to myopia and optic disc area: a quantitative and three-dimensional analysis. *BMC Ophthalmol*. 2017;17:22.
- 60. Lu B, Wang Y, Zhang P, et al. Evaluation of the association of macular ganglion cell-inner plexi-

translational vision science & technology-

- form layer thickness and myopia in Chinese young adults. *Eye* (*Lond*). 2021;35:393–399.
- 61. Khuu SK, Kalloniatis M. Spatial summation across the central visual field: implications for visual field testing. *J Vis.* 2015;15:6.
- 62. Khuu SK, Kalloniatis M. Standard automated perimetry: determining spatial summation and its effect on contrast sensitivity across the visual field. *Invest Ophthalmol Vis Sci.* 2015;56:3565.